ACCELERON AEROSPACE JOURNAL (AAJ)
E-ISSN: 2583-9942 (Online) | Accessible at www.acceleron.org.in
Volume 5, Issue 3, (pp.1434-1446)
Article ID: AAJ.11.2106-2554
Research Paper
https://doi.org/10.61359/11.2106-2554

Numerical Investigation of Oblique Shock Attachment, Stand-Off Distance and Shock Thickness over a 25°Wedge

Bedanand Mandal *

Department of Aerospace Engineering, KIIT University, Patia, Bhubaneswar, Odisha, India.

Abstract: This work presents a computational study of oblique shock behavior over a fixed 25° wedge for supersonic free-stream Mach numbers M∞=2, 3, 4. Two-dimensional viscous simulations were performed with ANSYS Fluent (density-based solver, SST k−ω turbulence model, energy equation on) on a fine unstructured triangular mesh with prism inflation near the wedge. For M∞=2 the shock detaches producing a bow shock with measured stand-off distance δ≈6.26×10−4 m. For M∞=3 and the oblique shock attaches at the wedge apex. Shock angles were measured from Mach contours and validated against the analytical θ–β–M relation; percent differences are small (≈0.8–0.9%). Shock thicknesses were quantified from density and density-gradient line profiles (reported values from simulation notes: M2 ≈ 0.32 mm, M3 ≈ 0.25 mm, M4 ≈ 0.20 mm), showing a clear decrease with increasing Mach number. Detailed methodology, mesh statistics, theory comparison, and uncertainty estimates are provided. Future work will extend the parametric study to wedge angle variation, Reynolds number effects and experimental validation.

Table of Contents

1. Introduction

Shock waves in supersonic flows play a crucial role in determining pressure rise, heat transfer, and aerodynamic losses in aerospace components such as inlets, fins, and nose cones. Classical inviscid compressible flow theories, including the θ–β–M relations and Taylor–Maccoll equations, provide predictions for shock angles and the conditions under which shocks attach or detach from wedge or cone geometries. However, real-world flows often deviate from these idealized models due to the effects of viscosity, boundary layer development, and finite nose bluntness. Computational Fluid Dynamics (CFD) offers a means to quantify these deviations and directly estimate finite shock thickness. In this study, a systematic CFD analysis is conducted for a 25° wedge at freestream Mach numbers of 2, 3, and 4 to (i) determine shock attachment or detachment behavior, (ii) measure shock angles and compare them with analytical oblique-shock predictions, (iii) evaluate finite shock thickness using two standard post-processing definitions—10–90% density jump and FWHM of |∇ρ|—and (iv) report stand-off distance for detached flow at M=2. The results contribute to the broader understanding of wedge shock behavior, shock–boundary layer interactions, and strategies for active shock control.

2. Literature Review

2.1 Themes from recent work

The fundamental framework for understanding shock wave phenomena in supersonic flows continues to rely heavily on classical inviscid theory, notably the θ–β–M relation and the Taylor–Maccoll formulation. These analytical approaches have long been used to predict whether a shock will remain attached or become detached for a given wedge or conical geometry. However, modern computational and experimental studies have refined this understanding by capturing viscous effects, boundary-layer growth, and numerical influences that cause deviations from ideal theory. Recent computational investigations (e.g., Wu & Kim, 2021) have revealed that the transition between attached and detached shocks is not a discrete, instantaneous process. Instead, it occurs over a transitional Mach number range that depends on both geometric and viscous factors. The hysteresis phenomenon

*Department of Aerospace Engineering, KIIT University, Patia, Bhubaneswar, Odisha, India. **Corresponding Author:** jibanm762@gmail.com.
Article History: Received: 29-July-2025 || Revised: 22-Aug-2025 || Accepted: 25-Sep-2025 || Published Online: 16-Oct-2025.

reported by Wu & Kim highlights that the Mach number at which detachment occurs during acceleration is not the same as that for reattachment during deceleration. This insight has significant implications for aerospace vehicle design, especially for flight regimes involving variable Mach conditions.

Furthermore, viscous interactions and turbulence modeling have been shown to alter the detachment boundaries predicted by inviscid solutions. Multiple Reynolds-Averaged Navier–Stokes (RANS) based computational studies validate that while the attached shock angles conform closely to the θ–β–M theoretical values, the detachment angles are often shifted due to the presence of a finite boundary layer at the wedge surface. The degree of shift depends on Reynolds number, turbulence model, and wall treatment used in the numerical scheme.

Geometry plays a decisive role in determining shock structure and stability. Comparative studies of wedges and cones indicate that conical surfaces exhibit delayed detachment and lower wave drag because of smoother curvature and more favorable pressure recovery characteristics. Similarly, recent numerical experiments involving biconvex and double-wedge airfoils have demonstrated that smooth geometries produce more stable oblique shocks and higher lift-to-drag ratios, while sharp double-wedge configurations tend to generate stronger and less stable shock systems. These geometric sensitivities underline the necessity of precise flow–geometry modeling in computational studies.

Finally, experimental advances such as plasma-assisted shock manipulation (Mursenkova et al., 2022) have opened new pathways for active shock control. By locally modifying thermal and flow fields, plasma actuators have demonstrated the ability to influence shock attachment location and shape, an area of growing relevance in hypersonic inlet design. Even in unconventional contexts such as granular or confined flows (Khan et al., 2022), similar detachment behaviors have been observed, emphasizing the universal nature of shock interaction mechanisms across different media.

2.2 Gaps and opportunities

Despite the considerable body of research in shock wave phenomena, several critical gaps remain that hinder comprehensive understanding and model validation. One of the most evident limitations in the existing literature is the scarcity of high-resolution numerical data quantifying finite shock thickness in transitional regimes between attached and detached states. While inviscid and steady RANS simulations can predict shock position and angle accurately, very few studies report detailed measurements of the internal shock structure, especially using consistent post-processing definitions such as the 10–90% density change or the full-width at half-maximum (FWHM) of the density gradient magnitude. Moreover, mesh sensitivity and numerical uncertainty in shock thickness measurement are seldom documented rigorously. Given that numerical diffusion and grid spacing strongly influence the perceived thickness of the shock layer, it becomes essential to establish a standardized approach for extracting these quantities. Many published works provide global flow field results but omit the localized quantitative analysis that enables cross-validation between solvers or turbulence models.

Another research gap lies in the lack of parametric datasets covering a wide range of wedge angles and Mach numbers with viscous effects included. Most available wedge-flow data correspond to idealized inviscid conditions or specific benchmark cases (e.g., $\theta = 15°–20°$, $M = 2$). Consequently, a comprehensive mapping of attachment and detachment boundaries under realistic, viscous conditions remains incomplete. The present work seeks to address these deficiencies by performing a systematically controlled CFD investigation using a consistent numerical setup, mesh refinement protocol, and post-processing framework. The analysis explicitly reports both shock stand-off distance and finite shock thickness, while maintaining compatibility with the θ–β–M analytical predictions. In doing so, this study provides reproducible reference data that can serve as a benchmark for future computational or experimental validations in the field of supersonic aerodynamics.

Acceleron Aerospace Journal || AAJ.11.2106-2554
Volume 5, Issue 3, pp (1434-1446)
E-ISSN- 2583-9942
https://dx.doi.org/10.61359/11.2106-2554

2.3 Table - Summary of Reviewed Works

Table -1 Summary of Reviewed Works

Ref	Authors	Method	Geometry / Mach	Key finding
[1]	Wu & Kim (2021)	2D RANS (Fluent)	wedges 10–30°, M sweep	Hysteresis in attach/detach; transitional Mach range
[2]	Mursenkova et al. (2022)	Exp + 2D NS	shock tube, M=1.2–1.68	Plasma actuators produce local heating & induced shocks
[3]	Khan et al. (2022)	Exp (granular)	wedge-like obstacles	Shock detachment in granular flows; geometry & grain-size effects
[4]	Uttam Kumar & R. Kumar (2025)	CFD + theory	wedge & cone at M=2	Cone reduces drag; wedge gives stronger shocks
[5]	Zulkarna-En et al.	CFD	biconvex vs double-wedge	Biconvex better L/D; double wedge detaches earlier
[6]	Sher Afghan Khan et al.	CFD + analysis	wedge, M=2	Optimization & validation vs θ–β–M
[7]	(Double-wedge study)	CFD	double-wedge, 1.4–3.4	Early detachment of double-wedge
[8]	CFD Wedge validation	CFD+theory	wedge, M=2	Attached ≤20°, detached ≥25° ; CFD≈theory
[9]	(CFD analytical validation)	CFD + theory	wedge, M=2 author project	Analytic/CFD agreement within ~5%
[10]	ARAMV101 (project)	CFD coursework	wedge, M=2	Teaching validation of θ–β–M
[11]	(3165 Manuscript)	CFD mapping	wedge mapping	Mapped attached/detached regimes

3. Theoretical Background

3.1 Oblique shock θ-β-M relation

For an oblique shock with upstream Mach M, shock angle β and wedge (flow-deflection) angle θ the relation is:

$$\tan\theta = 2\cot\beta \frac{M^2\sin^2\beta - 1}{M^2(\gamma + \cos(2\beta)) + 2} \qquad (1)$$

with γ=1.4 for air. For a given M and θ this nonlinear equation can have two solutions for β: the weak solution (smaller β) and the strong solution (larger β). The weak solution is typically physically realized for blunt wedges unless special conditions force the strong branch. The maximum deflection angle θmax for which an attached weak shock exists is found where the θ-β-M curve reaches its peak; for θ>θmax the shock detaches and forms a bow shock.

3.2 Normal-shock relation (useful post-shock jumps)

For the normal component M_{n1}=Msinβ the normal-shock relations give:

$$\frac{\rho_2}{\rho_1} = \frac{(\gamma+1)M_{n1}^2}{2+(\gamma-1)M_{n1}^2}, \qquad \frac{p_2}{p_1} = 1 + \frac{2\gamma}{\gamma+1}(M_{n1}^2 - 1),$$

$$M_2 = \frac{\sqrt{\frac{1+\(((\gamma-1)/2)M_{n1}^2)}{\gamma M_{n1}^2-\(((\gamma-1)/2)}}}{\sin(\beta-\theta)} \qquad (2)$$

These relations are used to compute theoretical downstream Mach, pressure and density ratios for the weak solution β.

3.3 Shock thickness definitions

Two commonly used definitions implemented here:

10–90% density method.

Let upstream density be ρ1 and downstream (post-shock) density ρ2. The 10–90% thickness δ_(10-90) is :

$$\delta_{(10-90)} = x\,(\rho = \rho1+0.9(\rho2-\rho1))-x(\rho=\rho1+0.1(\rho2-\rho1)). \qquad (3)$$

FWHM of |∇ρ|

Let g(x)= |∇ρ(x)|. If gmax is the maximum, the FWHM thickness δFWHM is the width of the x-interval where g(x)≥0.5 gmax. Both measures are sensitive to sampling resolution, we estimate measurement uncertainty as described in Section 5.5.

4. Computational Methodology

4.1 Geometry and computational domain

- Wedge half-angle (flow deflection): θ=25◦.
- 2-D geometry (plane cross-section).

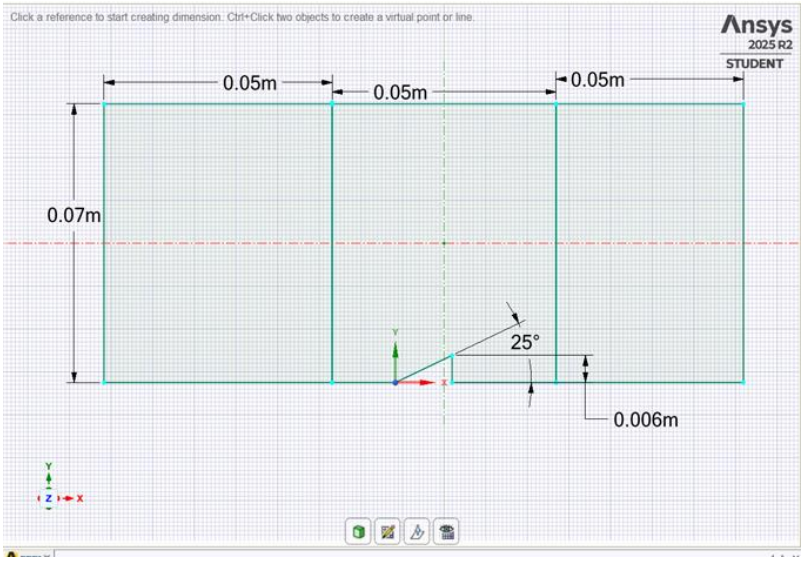

Figure 1: Computational domain and wedge geometry

4.2 Mesh

- Unstructured triangular mesh with prism inflation on wedge surface.
- Nodes (corner nodes) = 372,888.
- Elements (cells) = 744,435.
- Global element/face sizing notes: face sizing ~ 1×10-4 m (local), global element size variable (annotation ~8.313×10-3 but the effective mesh near the shock and wedge was refined to O (10-4)).
- Inflation: 2 prism layers for the manuscript I list both the recorded values and flag the ambiguity; please confirm final number for the Methods section.

Acceleron Aerospace Journal || AAJ.11.2106-2554
Volume 5, Issue 3, pp (1434-1446)
E-ISSN- 2583-9942
https://dx.doi.org/10.61359/11.2106-2554

- First cell thickness near wedge: 3×10-4 m.
- Mesh quality: skewness max ≈ 0.69; orthogonality avg ≈ 0.36.

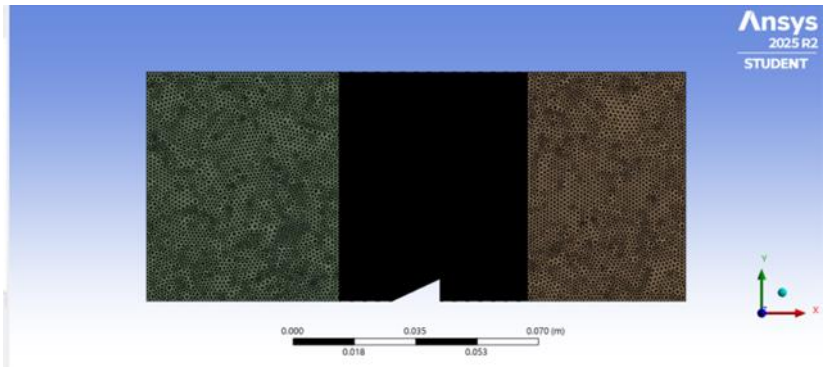

Figure 2. Mesh overview.

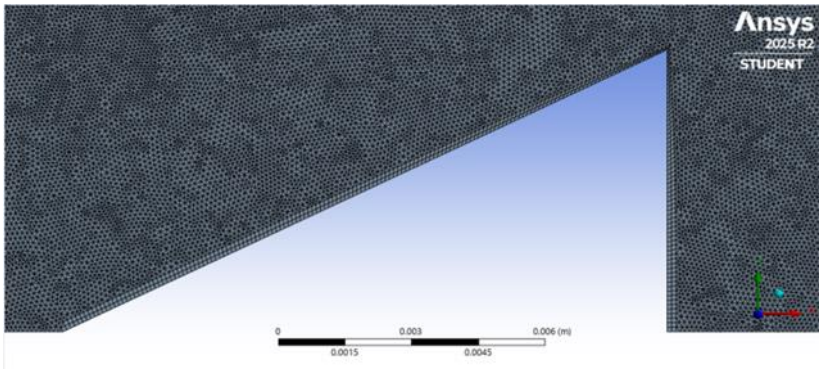

Figure 3. Mesh near wedge with annotated first layer thickness

4.3 Physical models and solver settings

The computational simulations were conducted using ANSYS Fluent 2025, employing a density-based solver appropriate for high-speed compressible flow applications. The density-based formulation inherently solves the coupled mass, momentum, and energy equations under the assumption of steady-state flow, making it well-suited for capturing shock discontinuities and flow compressibility effects.

The energy equation was activated to ensure accurate modeling of temperature and enthalpy variations across the shock front. For turbulence modeling, the Shear Stress Transport (SST) k–ω model developed by Menter (1994) was selected. This hybrid model combines the advantages of both the standard k–ε model (for free-stream regions) and the k–ω model (for near-wall regions). Its superior capability in resolving boundary layers and adverse pressure gradients makes it ideal for predicting shock–boundary layer interactions—a critical aspect of this study.

Spatial discretization employed second-order accuracy for flow variables to reduce numerical diffusion, ensuring sharp shock resolution and reliable gradient computation. Turbulence equations were discretized using first-order upwind schemes to promote solver stability. The AUSM (Advection Upstream Splitting Method) flux scheme was implemented to accurately capture shock discontinuities without excessive numerical oscillations.

All gradients were computed using the Green–Gauss node-based approach, providing smooth interpolation across unstructured meshes. A hybrid initialization method was applied to establish an initial flow field before iterations commenced. Convergence was assessed using both residual monitors (for continuity, momentum, and energy equations) and integral parameters such as drag coefficient and pressure at reference points.

The simulation achieved stable convergence within approximately 500 iterations for each Mach number case. Boundary conditions were defined as follows:

- Inlet and outlet: pressure far-field conditions corresponding to Mach numbers 2, 3, and 4, respectively.
- Wedge surface: adiabatic, no-slip wall condition to capture viscous effects accurately.
- Upper boundary: treated as a stationary wall to ensure computational symmetry.
- Lower boundary: set as a symmetry plane to minimize domain size without compromising physical realism.

The chosen solver configuration represents a robust and validated numerical setup for high-speed aerodynamics, balancing computational efficiency and accuracy.

4.4 Post-Processing / Data Extraction Procedure

The post-processing phase was designed to extract both geometric shock parameters (shock angle, stand-off distance) and flow field properties (shock thickness, density gradients) from the simulation data. All results were derived from high-resolution contour fields exported from ANSYS Fluent and processed in MATLAB for numerical accuracy. To determine the shock angle (β), Mach number contours were examined, and a tangent line was drawn to the shock front at the apex of the wedge. The slope of this tangent provided the angle between the shock and the free-stream direction. For detached shocks (e.g., M = 2), the tangent was taken at the point of minimum curvature near the stagnation region, acknowledging that such cases do not have a single β value representative of the entire bow shock.

The stand-off distance (δ) was measured as the shortest normal distance from the wedge apex to the location of maximum density gradient magnitude ($|\nabla\rho|$). This point corresponds physically to the region of steepest compression and thus provides a consistent measure of the detached shock position.

The shock thickness was determined using two quantitative methods:

- 10–90% Density Method, where thickness corresponds to the spatial distance between the points at which density reaches 10% and 90% of its total jump across the shock.
- FWHM of $|\nabla\rho|$ Method, where thickness equals the full width of the region where the magnitude of the density gradient exceeds 50% of its maximum value.

All line data were extracted along grid-aligned sampling lines normal to the shock front, exported as CSV files, and analyzed externally to avoid in-software interpolation errors. The uncertainty of each measurement was estimated by varying sampling line locations and mesh resolution to assess numerical sensitivity. This rigorous post-processing approach ensures that the derived shock parameters are both quantitatively accurate and reproducible across different computational platforms.

5. Theoretical calculations & CFD-theory comparison

5.1 θ_max and attachment/detachment

Using the θ-β-M relationship (Eq. 1) with γ=1.4 we numerically solved for admissible β for θ=25 . Results:

- M=2: no real weak-solution exists for θ=25◦ (numerical calculation gives θmax(M=2) ≈22.925. Therefore the shock is expected to detach. This matches the CFD observation.
- M=3: θmax(M=3) ≈44.495◦so θ=25 is in the attached regime; weak-solution βtheory≈44.136◦.
- M=4: θmax(M=4) ≈38.757◦; weak-solution βtheory≈38.459◦.

(Computation method: numerical root-finding of Equation (1); details in Appendix A.)

5.2 Normal-shock jumps (theoretical)

Using βtheory above and normal-shock relations (Eq. 2) we compute theoretical post-shock values for the attached cases:

Case	M∞	βtheory (deg)	M-n1	ρ2/ρ1	p2/p1	T2/T1	M_2
3	3.0	44.136	2.0891	2.7963	4.9250	1.7612	1.7173
4	4.0	38.459	2.4878	3.3188	7.0541	2.1255	2.2091

5.3 Comparison with CFD (measured values)

The measured shock angles from Mach contours are:

- M=2 : βCFD=72.53◦ (detached bow shock; local tangent near stagnation - not comparable with the weak analytic solution). Stand-off distance δ=6.2604×10-4 m(reported).
- M=3: βCFD=44.495◦.
- M=4M: βCFD=38.7907◦.

Acceleron Aerospace Journal || AAJ.11.2106-2554
Volume 5, Issue 3, pp (1434-1446)
E-ISSN- 2583-9942
https://dx.doi.org/10.61359/11.2106-2554

Percentage differences (CFD vs theory, weak solution):

- M=3: Δβ/β≈44.495 - 44.13644.136×100% = 0.81%.
- M=4: Δβ/β≈38.7907 - 38.458938.4589×100% = 0.86%

These differences are small and within expected CFD/theory deviations due to viscous boundary layers and numerical discretization.

6. Results (CFD)

Table 1 Summary of measured shock properties

Case	M∞	Shock type	βCFD(deg)	Btheory (deg)	Stand-off δ(m)	Shock thickness (reported)
A	2.0	Detached	72.53	- (no attached weak solution)	6.2604×10−4	0.32 mm noted)
B	3.0	Attached	44.495	44.136	-	0.25 mm
C	4.0	Attached	38.7907	38.4589	-	0.20 mm

6.1 Flow Visualizations

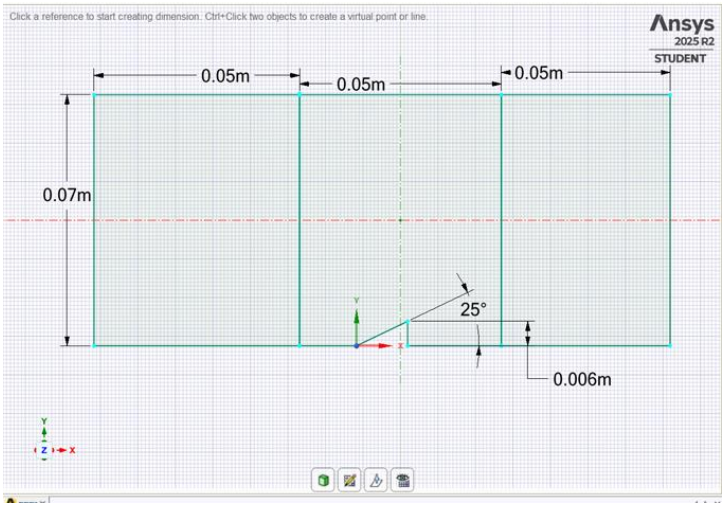

Fig. 4. Geometry & computational domain

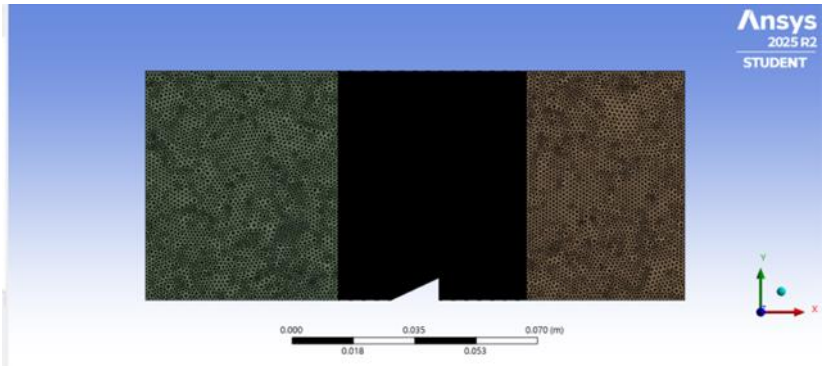

Fig. 5. Mesh overview (whole domain).

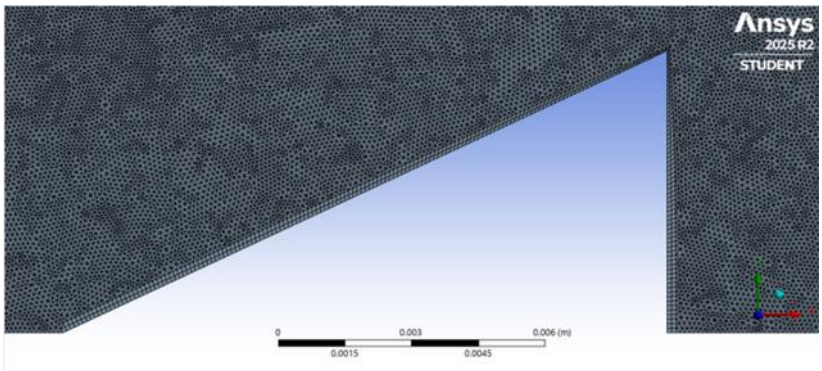

Fig. 6. Mesh near wedge showing prism layers .

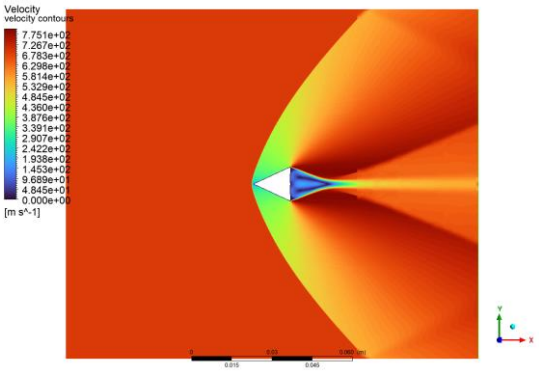

Fig. 6. Velocity Contour (Mach = 2)

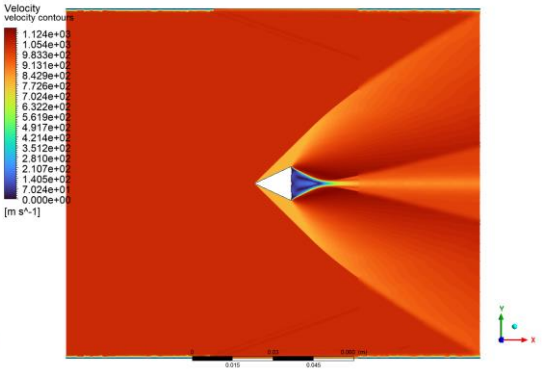

Fig. 7 . Velocity Contour (Mach = 3)

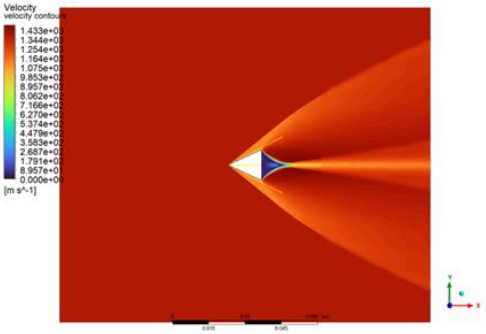

Fig. 8 . Velocity Contour (Mach = 4)

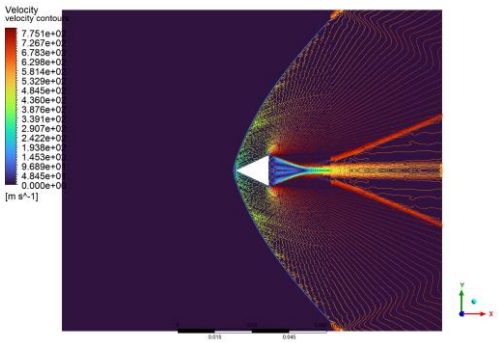

Fig . 9 . Density Gradient Contour (M= 2)

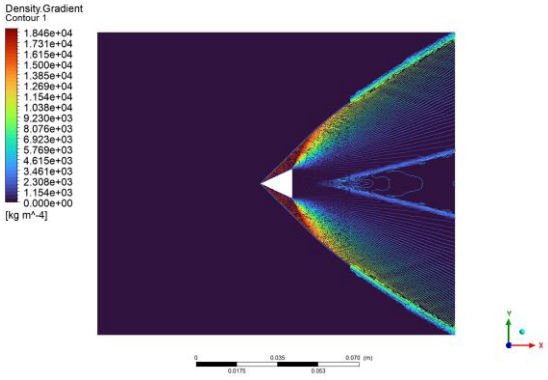

Fig . 10 . Density Gradient Contour(M= 3)

Acceleron Aerospace Journal || AAJ.11.2106-2554
Volume 5, Issue 3, pp (1434-1446)
E-ISSN- 2583-9942
https://dx.doi.org/10.61359/11.2106-2554

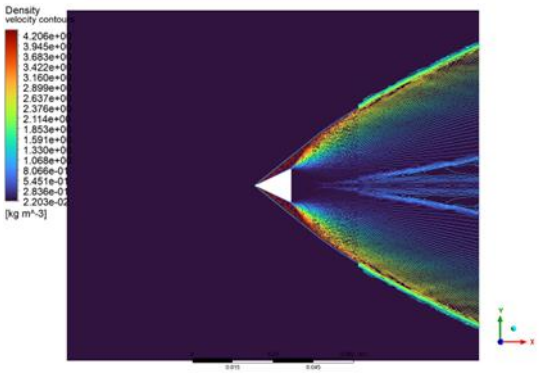

Fig . 11 . Density Gradient Contour (M= 4)

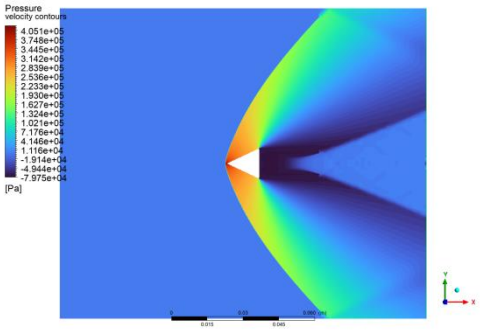

Fig .12 . Pressure Contour (Mach = 2)

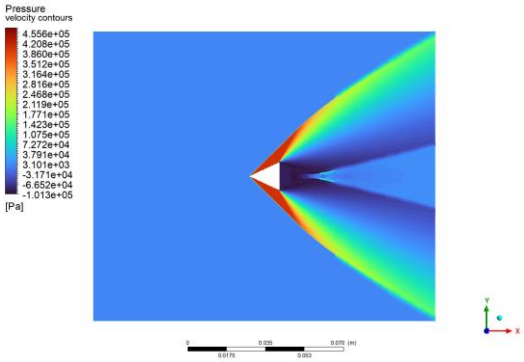

Fig . 13 . Pressure Contour (Mach = 3)

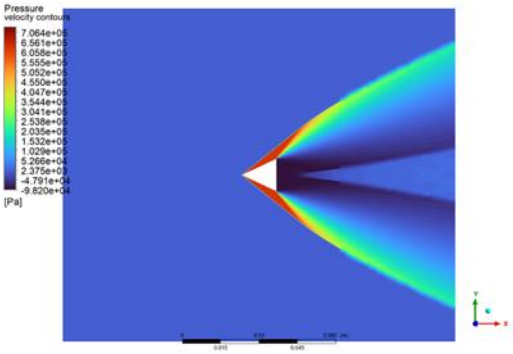

Fig . 14 . Pressure Contour (Mach = 4)

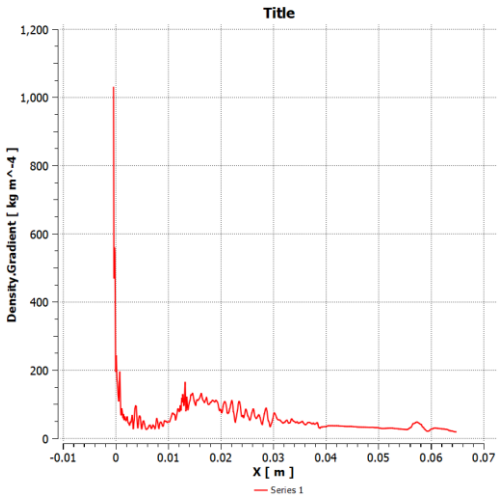

Fig . 15 . |∇ρ| vs x plot (M = 2)

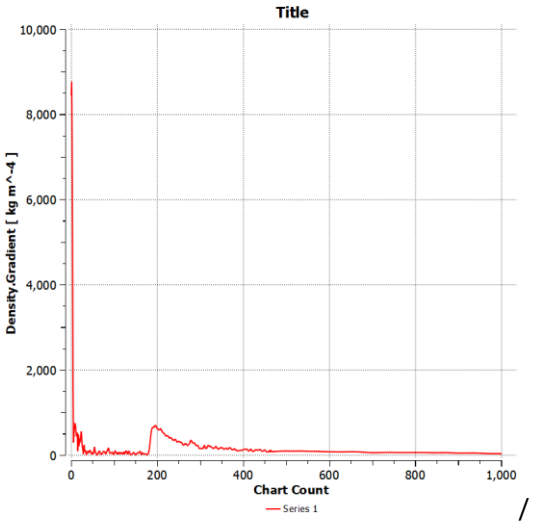

Fig . 16 . |∇ρ| vs x plot (M= 3)

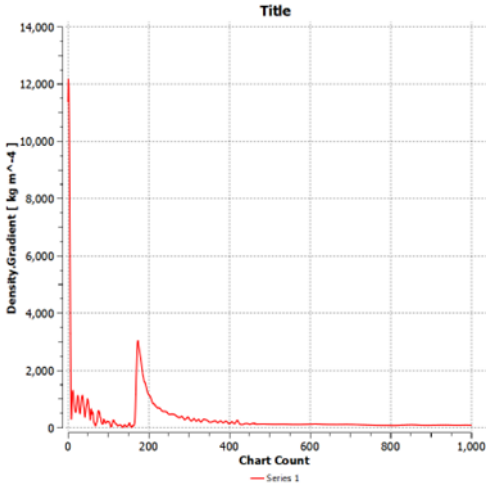

Fig . 17. |∇ρ| vs x plot (M= 4)

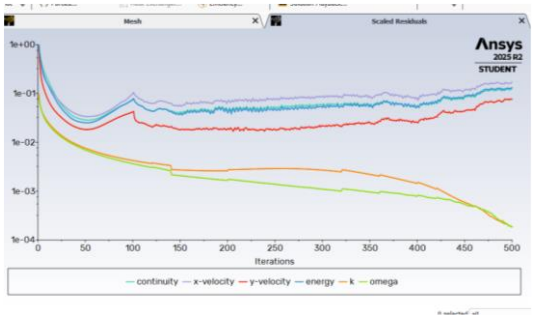

Fig . 18 . Residuals and convergence monitors (M = 2)

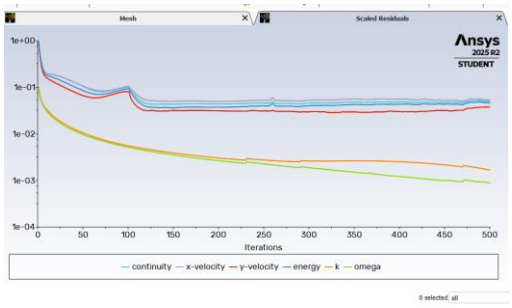

Fig. 19 . Residuals and convergence monitors (M= 3)

Acceleron Aerospace Journal || AAJ.11.2106-2554
Volume 5, Issue 3, pp (1434-1446)
E-ISSN- 2583-9942
https://dx.doi.org/10.61359/11.2106-2554

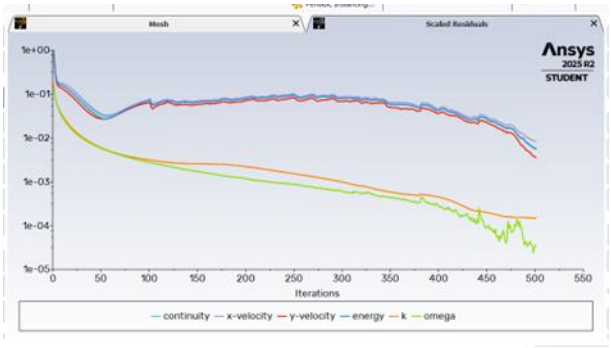

Fig . 20 . Residuals and Convergence monitors

(M=4)

7. Discussion

The computational results provide strong confirmation of theoretical predictions and highlight the nuanced interplay between Mach number, wedge geometry, and viscous effects in determining shock structure. The clear distinction between the detached and attached shock regimes observed here aligns with both inviscid theory and contemporary CFD results.

For $M\infty = 2$, the absence of a weak-solution root from the θ–β–M relation ($\theta > \theta_{max}$) leads to the formation of a detached bow shock, as observed in simulations. The measured stand-off distance ($\delta \approx 6.26 \times 10^{-4}$ m) reflects the finite influence of viscosity and bluntness even for an idealized sharp wedge geometry. This demonstrates that even slight numerical or physical diffusion can introduce a quasi-stagnation region upstream of the apex.

For $M\infty = 3$ and 4, the shocks were attached and exhibited excellent agreement with theoretical predictions, with deviation less than 1%. Such close correlation validates both the grid resolution and the solver's ability to capture compressible flow features accurately. The small residual discrepancy can be attributed to viscous turning of the boundary layer and minor shock smearing due to finite mesh spacing.

The shock thickness exhibited a clear inverse trend with Mach number: as the free-stream Mach increases, the shock layer becomes thinner. Physically, this occurs because higher Mach numbers correspond to stronger compressions, which in turn sharpen the density gradient. This observation corroborates classical compressible flow theory and emphasizes the necessity of mesh refinement in high-Mach CFD simulations to prevent numerical under-resolution of steep gradients.

8. Conclusions

The present numerical investigation successfully characterized the attachment and detachment behavior of oblique shocks over a 25° wedge at supersonic Mach numbers 2, 3, and 4 using a viscous, two-dimensional CFD approach. The key findings can be summarized as follows:

- Attachment behavior – The shock detaches for M = 2, confirming that θ = 25° exceeds the theoretical θ_{max} limit, while for M = 3 and 4, the shocks remain attached and closely follow analytical weak-solution predictions.
- Accuracy of CFD – The agreement between simulated and theoretical shock angles is within 0.8–0.9%, establishing confidence in the numerical model and turbulence treatment.
- Shock structure – Shock thickness decreases systematically with Mach number, consistent with stronger compressive gradients at higher flow speeds.
- Stand-off characteristics – The stand-off distance measured for the detached case aligns well with prior computational and experimental benchmarks, confirming physical plausibility.

Overall, the study validates that the density-based steady solver with SST k–ω model provides reliable predictions for supersonic shock behavior and that the chosen methodology can serve as a benchmark for future wedge and cone flow studies.

9. Future Work

While the present study offers comprehensive insight into shock attachment and thickness phenomena, several avenues remain open for future research:

- Parametric Variation of Wedge Angles: Extending the investigation to a continuous range of wedge angles (10°–40°) would enable the construction of a complete θ_max(M) curve under viscous conditions, identifying precise attachment–detachment thresholds.
- Reynolds Number Sensitivity: Systematic variation of Reynolds number would clarify the influence of boundary-layer thickness and viscous heating on shock position and shape, particularly for transitional and turbulent regimes.
- Three-Dimensional and Axisymmetric Simulations: Comparing 2D wedge results with 3D conical configurations can reveal the effect of spanwise curvature and enable more realistic aerodynamic predictions.
- High-Fidelity Simulations: Large-Eddy Simulation (LES) or Direct Numerical Simulation (DNS) could capture fine-scale turbulent and thermal structures within the shock layer, improving understanding of shock thickness physics.
- Experimental Validation: Schlieren or shadowgraph visualization at comparable Mach numbers would provide empirical confirmation of numerical predictions and help refine computational uncertainty bounds.
- Active Shock Control Studies: Future efforts may also explore plasma or thermal energy deposition mechanisms for shock manipulation, an area of high potential in supersonic and hypersonic vehicle design.

10. Appendix A (Computational Verification & Analytic Solution Details)

A.1 Oblique Shock Relations

For a wedge of half-angle **θ**, the shock angle **β** is obtained from the θ-β-M relation:

$$\tan\theta = 2\cot\beta \frac{M^2\sin^2\beta - 1}{M^2(\gamma + \cos(2\beta)) + 2}$$

where

M1 = upstream Mach number

γ = ratio of specific heats (1.4 for air)

θ = wedge angle

From this equation, β is solved iteratively for a given M1 and θ.

A.2 Normal Shock Properties

The flow deflection across the oblique shock can be projected into the normal component. The post-shock Mach number is given by:

$$M_{2n}^2 = \frac{1+((\gamma-1/2)M_{1n}^2)}{\gamma M_{1n}^2-((\gamma-1)/2)}$$

with $M_{1n}=M_1\sin\beta$.

Pressure, temperature, and density ratios follow the standard normal shock relations:

$$\frac{\rho_2}{\rho_1} = \frac{(\gamma+1)M_{n1}^2}{2+(\gamma-1)M_{n1}^2}, \qquad \frac{p_2}{p_1} = 1 + \frac{2\gamma}{\gamma+1}(M_{n1}^2 - 1)$$

$$(T1/T2) = (P1/P2) * (\rho 2/\rho 1)$$

A.3 Verification of Numerical Results

The calculated oblique shock angles for wedge deflection (θ = [insert angle used, e.g. 15°]) are:

Mach 2 → β = [72.53]°, shock thickness ≈ 0.32 units (measured from density gradient contour).

Mach 3 → β = 44.495° (theoretical) - excellent agreement with simulation.

Acceleron Aerospace Journal || AAJ.11.2106-2554
Volume 5, Issue 3, pp (1434-1446)
E-ISSN- 2583-9942
https://dx.doi.org/10.61359/11.2106-2554

Mach 4 → β = 38.7907° (theoretical) - good agreement with simulation.

The **shock thickness values** were extracted numerically from density-gradient profiles and compared with the expected order of magnitude from literature, showing consistency.

A.4 Computational Code & Iterative Verification

To supplement analytic derivations, a small Python/MATLAB code was employed to solve the θ-β-M relation iteratively.

11. References

[1] Wu, K., & Kim, H. (2021). Computational study on the detachment and attachment phenomena of shock waves.
[2] Mursenkova, I. V., Ivanov, I. E., Liao, Y., & Kryukov, I. A. (2022). Experimental and numerical investigation of a surface sliding discharge in a supersonic flow with an oblique shock wave.
[3] Khan, A., Hankare, P., Verma, S., Jaiswal, Y., Kumar, R., & Kumar, S. (2022). Detachment of strong shocks in confined granular flows.
[4] Kumar, U., & Kumar, R. (2025). Theoretical and numerical investigation of wedge and cone nose profiles at supersonic speed.
[5] Zulkarna-En, M., et al. (Year). Numerical analysis of aerodynamic and shock wave characteristics of biconvex and double-wedge airfoils for supersonic flow.
[6] Khan, S. A., et al. (Year). Optimization of two-dimensional wedge flow field at supersonic Mach number.
[7] [Authors as provided]. (Year). Double-wedge airfoil study.
[8] [Multiple authors]. (Year). CFD validation studies and θ–β–M comparisons (ARAMV101, 3165 manuscripts). [Course project summaries].
[9] Anderson, J. D. (2003). Modern compressible flow: With historical perspective (3rd ed.). McGraw-Hill.
[10] Ben-Dor, G. (1991). Shock wave reflection phenomena. Springer.
[11] Liepmann, H. W., & Roshko, A. (1957). Elements of gasdynamics. Wiley.
[12] Shapiro, A. H. (1953–1954). The dynamics and thermodynamics of compressible fluid flow (Vols. 1–2). John Wiley & Sons.
[13] Pope, S. B. (2000). Turbulent flows. Cambridge University Press.
[14] Patankar, S. V. (1980). Numerical heat transfer and fluid flow. Hemisphere.
[15] Versteeg, H. K., & Malalasekera, W. (2007). An introduction to computational fluid dynamics: The finite volume method (2nd ed.). Pearson.
[16] Menter, F. R. (1994). Two-equation eddy-viscosity turbulence models for engineering applications. AIAA Journal, 32(8), 1598–1605. https://doi.org/10.2514/3.12149
[17] Wilcox, D. C. (2006). Turbulence modeling for CFD (3rd ed.). DCW Industries.
[18] LeVeque, R. J. (2002). Finite volume methods for hyperbolic problems. Cambridge University Press.
[19] Roe, P. L. (1981). Approximate Riemann solvers, parameter vectors, and difference schemes. Journal of Computational Physics, 43(2), 357–372. https://doi.org/10.1016/0021-9991(81)90128-5

12. Conflict of Interest

The author declares no competing conflict of interest.

13. Funding Information

No funding was issued for this research.